Relic neutrino background from cosmic-ray reservoirs

Andrea Giovanni De Marchi,[*] Alessandro Granelli,[†] Jacopo Nava,[‡] and Filippo Sala[§,¶]

Dipartimento di Fisica e Astronomia, Università di Bologna, via Irnerio 46, 40126, Bologna, Italy and INFN, Sezione di Bologna, viale Berti Pichat 6/2, 40127, Bologna, Italy

(Received 20 May 2024; revised 22 July 2024; accepted 17 December 2024; published 10 January 2025)

We compute the flux of relic neutrino background (RνB) up-scattered by ultrahigh-energy (UHE) cosmic rays (CRs) in clusters that act as CR-reservoirs. The long trapping times of UHECRs make this flux larger than that of RνB up-scattered by UHECRs on their way to Earth, which we also compute. We find that IceCube excludes RνB weighted overdensities larger than 10^{10} in clusters, and that PUEO, RNO-G, GRAND, and IceCube-Gen2 will test values down to 10^{8}. Our treatment incorporates the momentum transfer dependence of the neutrino-nucleus cross section, deep inelastic scattering, a mixed UHECR composition, and flavor information on the up-scattered RνB fluxes for both cases of neutrino mass spectrum with normal and inverted ordering, providing new handles to possibly disentangle the up-scattered RνB from cosmogenic neutrinos.

DOI: 10.1103/PhysRevD.111.023023

I. INTRODUCTION

The relic neutrino background (RνB) is referred to as the "Holy Grail" of neutrino physics. It is the only subcomponent of dark matter that is predicted by the standard cosmological model (ΛCDM), with a present temperature and number density per-flavor (counting neutrinos and antineutrinos separately) of [1]

$$T_{\nu,0} \simeq 1.67 \times 10^{-4}\ \text{eV}, \qquad n_{\nu,0} \simeq 56\ \text{cm}^{-3}. \tag{1}$$

Its detection would give new observational access to the earliest cosmological times ever probed. We have indirect evidence for it via early Universe observations [2,3], but none of the existing techniques to detect the local RνB is expected to discover it in the foreseeable future, see [4] for a recent overview. It has been furthermore pointed out that PTOLEMY [5,6], which aims at detecting the RνB by capture on tritium, is insensitive to it, if graphene is used to stock tritium, because of Heisenberg uncertainty [7,8]. Experiments aiming at detection of the local RνB then only test the case where its local density is much larger than the diffuse cosmological one $n_{\nu,0}$ by an overdensity factor $\eta_\nu^{\text{Earth}} > 1$. The strongest such limit has been set by the KATRIN experiment [9] and reads $\eta_\nu^{\text{Earth}} < 1.3 \times 10^{11}$, in the same ballpark of limits from the RνB gravitational effects in the Solar System [10]. Given that gravitational clustering can induce at most $\eta_\nu^{\text{Earth}} \sim 10^2$ [11], these experiments then only test the beyond the Standard Model (BSM) scenarios, if any, that lead to those large local overdensities.

The main challenge to detect the RνB is its tiny energy, as a consequence of its low temperature $T_{\nu,0}$. A possible way-out consists in looking for consequences of the highest-energy scatterings that the RνB can undergo in the Universe, so to maximize their SM cross sections. To our knowledge, the first exploration along these lines was the computation of the RνB flux up-scattered by ultrahigh-energy (UHE) cosmic rays (CRs), carried out by Hara and Sato in the 1980s [12,13], when much less than today was known about both neutrinos and UHECRs. This idea has been dormant for forty years, until the authors of [14] revived it and, from the nonobservation of such an up-scattered RνB flux at IceCube, constrained overdensities in the ballpark of $10^{13}(10^{11})$ on scales of about 10 kpc in the Milky Way (around the blazar TXS $0506+056$). While the study [14] is sufficient to set a rough limit, it has limitations, like assuming that all UHECRs are protons (which we know is not the case [15,16]), as well as using an oversimplified SM cross section. These should be addressed in order to possibly hope to detect the

[*]Contact author: andreagiovanni.demarchi@unibo.it
[†]Contact author: alessandro.granelli@unibo.it
[‡]Contact author: jacopo.nava2@unibo.it
[§]Contact author: f.sala@unibo.it
[¶]On leave from LPTHE, CNRS, and Sorbonne Université, Paris, France.

up-scattered RνB flux and disentangle it from other neutrinos that could show up in a similar energy range, like cosmogenic ones.[1]

The RνB overdensities tested by the techniques above are not only considerably larger than those achievable via gravitational clustering [11], but also violate the Pauli exclusion principle unless one introduces BSM physics that would cluster the RνB more than gravity, see [24] for a systematic assessment. To our knowledge, the largest overdensities achieved in a fully worked-out BSM model rely on a tiny long-range neutrino self-interaction [25]. They read $\eta_\nu^{\rm BSM} \simeq 10^7 (m_\nu/0.1\ {\rm eV})^3$, where m_ν is the neutrino mass scale, and extend up to a volume of the size of a galaxy cluster, motivating to test large overdensities in these environments.

In this manuscript, we propose to look for the RνB up-scattered by UHECRs in clusters that act as CR-reservoirs [26–32] and calculate the associated fluxes. This idea benefits from the long trapping times of CRs in these environments, and from the knowledge on them that is available today and will increase with upcoming observations in the near future. Additionally, we improve over [14] in the calculation of UHECR-up-scattered RνB fluxes in a number of ways, which we will show to be quantitatively important.

II. UP-SCATTERING THE RELIC NEUTRINO BACKGROUND WITH COSMIC RAYS

The flux of accelerated relic neutrinos per unit energy E_ν, from the up-scattering environments of interest, can be written as

$$\frac{d\Phi_\nu}{dE_\nu} = D_{\rm eff} n_{\nu,0} \bar{\eta}_\nu \int_{E_{\rm CR}^{\rm min}(E_\nu)}^{E_{\rm CR}^{\rm max}} dE_{\rm CR} \frac{d\Phi_{\rm CR}}{dE_{\rm CR}} \frac{d\sigma_{\nu{\rm CR}}}{dE_\nu}, \quad (2)$$

where the effective distance $D_{\rm eff}$ contains information on the spatial distribution of relic neutrinos and CRs; $\bar{\eta}_\nu \equiv (1/V)\int_V d^3\vec{r}\eta_\nu(\vec{r})$ is the RνB overdensity averaged over the volume V, with $\eta_\nu(\vec{r}) = n_\nu(\vec{r})/n_{\nu,0}$ and $n_\nu(\vec{r})$ being the neutrino number density at position $\vec{r}$; $E_{\rm CR}^{\rm min}(E_\nu)$ is the greatest value between the minimal available CR energy and the lowest energy required by the kinematics of the scattering; $E_{\rm CR}^{\rm max}$ is the largest CR energy in their flux; $d\Phi_{\rm CR}/dE_{\rm CR}$ is the CR flux per unit of CR energy $E_{\rm CR}$; $d\sigma_{\nu{\rm CR}}/dE_\nu$ is the differential cross section for the ν-CR scattering. The dependence on the up-scattering environment, in this letter either the Milky Way or CR-reservoirs, is contained in $D_{\rm eff}$ and $d\Phi_{\rm CR}/dE_{\rm CR}$. The total neutrino flux is understood to be the sum of Eq. (2) over all neutrinos and nuclear species composing CRs.

A. Neutrino-nucleus scattering at UHEs

We consider the up-scattering of a relic (anti)neutrino ν ($\bar{\nu}$) by a cosmic nucleus $\mathcal{N}$ via pure SM neutral current (NC) interaction. At the ν-$\mathcal{N}$ exchanged energies that we are interested in, the scattering is described by that on the nucleons $N = p, n$ as

$$\frac{d\sigma_{\nu\mathcal{N}}}{dE_\nu}(E_\mathcal{N}) \simeq \frac{A_\mathcal{N}}{2}\left[\frac{d\sigma_{\nu p}}{dE_\nu}\left(\frac{E_\mathcal{N}}{A_\mathcal{N}}\right) + \frac{d\sigma_{\nu n}}{dE_\nu}\left(\frac{E_\mathcal{N}}{A_\mathcal{N}}\right)\right], \quad (3)$$

where we have focused for simplicity on isoscalar nuclei with equal number $A_\mathcal{N}/2$ of protons and neutrons, each carrying a fraction $1/A_\mathcal{N}$ of the nucleus's energy $E_\mathcal{N}$, and summed over elastic scattering (ES) and deep inelastic scattering (DIS) contributions: $d\sigma_{\nu N}/dE_\nu = d\sigma_{\nu N}^{\rm ES}/dE_\nu + d\sigma_{\nu N}^{\rm DIS}/dE_\nu$. The ES part, summed over ν and $\bar{\nu}$, reads [33,34]

$$\frac{d\sigma_{\nu N}^{\rm ES}}{dE_\nu} = \frac{2G_F^2 m_\nu m_N^4}{\pi(s-m_N^2)^2}\left[A_N(Q^2) + C_N(Q^2)\frac{(s-u)^2}{m_N^4}\right], \quad (4)$$

where G_F is the Fermi constant; $s = 2m_\nu E_N + m_N^2 + m_\nu^2$, $Q^2 = 2m_\nu(E_\nu - m_\nu)$ is the momentum transfer squared, $u = 2m_\nu^2 + 2m_N^2 - s + Q^2$; $m_{N(\nu)}$ is the nucleon (neutrino) mass and $E_{N(\nu)}$ is the energy of the incoming nucleon (outgoing neutrino) in the frame in which the initial neutrino is at rest. The functions A_N and C_N are given in Appendix A (see, e.g., [33,34]) and strongly suppress ES for $Q^2 \gtrsim m_N^2 \approx {\rm GeV}^2$. The DIS, in which the initial neutrino interacts directly with the quark constituents of the nucleons, takes over for $E_N \gtrsim 10^{10-11}$ GeV, given $Q^2 \lesssim s$ and $m_\nu \approx 0.1$ eV, thus being necessary to describe the highest-energy part of the up-scattered RνB flux. For the NC ν-N DIS cross section we adopt

$$\frac{d\sigma_{\nu N}^{\rm DIS}}{dE_\nu} \simeq \sum_{a=q,\bar{q}} \frac{G_F^2[(g_V^a)^2 + (g_A^a)^2]}{2\pi E_N} \times \int_{y_{\rm min}}^1 \frac{dy}{y^2}\frac{Q^2 f_a^N(x,Q^2)}{[1+Q^2/M_Z^2]^2} g(y,Q^2,m_N), \quad (5)$$

where $g(y,Q^2,mN) \equiv (y^2 - 2y + 2 - 2m_N^2 x^2 y^2/Q^2)$, M_Z is the Z boson mass, y is the inelasticity parameter satisfying $y_{\rm min} = (E_\nu - m_\nu)/E_N \lesssim y \le 1$, $x = (E_\nu - m_\nu)/(E_N y)$ is the Bjorken scaling variable and $f_a^N(x,Q^2)$ is the parton distribution function (PDF) for the quark a having NC vector and axial coupling g_V^a and g_A^a, $a = u, d, s, c, b$ (we neglect any contribution from the top quark). We evaluate the PDFs with the Python package `parton` using the "CT10" PDF set [35] (see also this website for more details). For simplicity,

[1]The RνB could also be indirectly tested via features that its scatterings induce in UHE neutrinos on their way to Earth [17,18]. IceCube observations constrain this way $\eta_\nu \lesssim 10^{11}(10^8)$ on scales of 10 kpc (of the 14 Mpc that separate us from NGC 1068) [19]. Resonant dips in UHE cosmogenic neutrinos [20], not observed so far [21,22], could at best test $\eta_\nu \sim 10^{11}$ on scales of the entire Universe [23], which are already ruled-out by not overclosing it.

we do not take the coherent ν-$\mathcal{N}$ scattering into account as it could contribute only at energy scales smaller than those of interest to our study [34,36], and neglect the contribution to $d\sigma_{\nu\mathcal{N}}/dE_\nu$ from hadronic resonances [37,38], relevant for $Q^2 \approx \mathrm{GeV}^2$, so that in the considered range our results are conservative. Details on the derivation of Eq. (5) are given in Appendix B.

B. CRs up-scattering RνB *en route* to Earth

As they travel toward the Earth, UHECRs up-scatter the RνB with the largest cross sections among all CRs, and induce a flux described by Eq. (2). While the bulk of CRs with energy much below the EeV are believed to originate within the Milky Way (MW) [39,40] and to be mostly protons below the PeV [41], UHECRs above the EeV scale are today understood as having an extragalactic origin, see e.g., [42–44], and a mixed composition with heavier nuclei dominating over protons, see, e.g., [15,16,45–50]. We therefore employ the CR spectrum $d\Phi_{\rm CR}/dE_{\rm CR}$ from [15] and, by considering up-scatterings in the MW with the line-of-sight integral $D_{\rm eff} \approx 10$ kpc as in [14] (see, e.g., [51–53] for studies of the uncertainties on $D_{\rm eff}$, where the RνB case is analogous to relativistic DM fluxes and cored profiles like Isothermal), we obtain the flux reported as a dot-dashed line in Fig. 1 (see further). Our calculation improves over the analogous one [14] by going beyond the proton-only composition of CRs and by implementing the momentum transfer dependence and DIS in the cross section. It results in a significantly different flux with respect to [14], see Appendix C for details of the comparison.

Since tentative sources of UHECRs are located at 1–100 Mpc from Earth [65–69], $D_{\rm eff}$ can be larger than 10 kpc by orders of magnitude, resulting in a sensitivity to $\bar{\eta}_\nu \sim 10^{10-11}$. Still, these enormous $\bar{\eta}_\nu$ over such long distances are hard to justify without spoiling the large-scale homogeneity of the Universe, motivating us to look for environments where $D_{\rm eff}$ can be sizeable while keeping neutrino overdensities localized on smaller scales.

C. Boosted RνB from CR-reservoirs

A possible explanation for the extragalactic origin of UHECRs is that they are produced inside galaxy clusters, in which they reside up to cosmological times before escaping and contributing to the UHECR flux on Earth [26–32] (see also [70] for a review). The distance they travel inside these gigantic CR-reservoirs would be roughly $c\tau_{\rm esc} \simeq 0.3\ \mathrm{Gpc}(\tau_{\rm esc}/1\ \mathrm{Gyr})$, where $\tau_{\rm esc}$ is the time CRs spend in the cluster before their release. The effective distance entering Eq. (2) can be written as $D_{\rm eff} = \mathcal{B} c\tau_{\rm esc}$, having defined the spatial boost factor

$$\mathcal{B} \equiv \int_V d^3\vec{r} f_{\rm CR}(x)\delta_\nu(\vec{r}), \tag{6}$$

with $\delta_\nu(\vec{r}) \equiv \eta_\nu(\vec{r})/\bar{\eta}_\nu$ and $f_{\rm CR}(\vec{r})$ the spatial profile of the CR flux inside a CR-reservoir of volume V, normalized

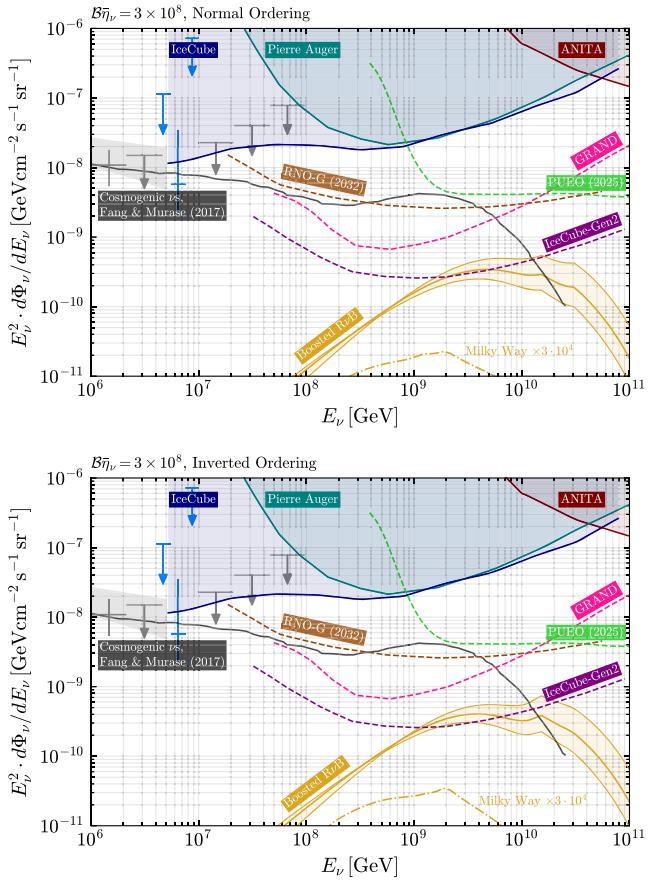

FIG. 1. All-flavor RνB fluxes on Earth as up-scattered by UHECRs inside galaxy clusters acting as CR-reservoirs (continuous gold lines) or from UHECRs in the MW (dot-dashed gold line, multiplied by 3×10^4). The yellow shaded region is obtained for $2 \le \alpha \le 2.5$ (central thick line, $\alpha = 2.3$), a weighted RνB overdensity $\mathcal{B}\bar{\eta}_\nu = 3\times10^8$, a neutrino mass spectrum with NO (IO) in the upper (lower) panel and $\sum_i m_i = 0.113(0.145)$ eV [54]. In gray and azure are the astrophysical neutrinos events observed at IceCube [55,56] (see also [57,58], the KM3NeT ARCA detector will have a similar sensitivity [59]). Fluxes of UHE neutrinos lying in the upper shaded regions are excluded at 90% confidence level (CL) by the null-detection at IceCube [21], Pierre Auger Observatory [22] and ANITA [60]. Sensitivities of PUEO (2025) [61], RNO-G (2032, first stations already taking data) [62], IceCube-Gen2 [63] (planned) and GRAND [64] (proposed) are depicted as dashed lines. The black line displays the cosmogenic neutrino flux from [31].

such that $\int_V d^3\vec{r} f_{\rm CR}(\vec{r}) = 1$. One has $\mathcal{B} = 1$ for a homogeneous RνB, $\delta_\nu(\vec{r}) = 1$, while $\mathcal{B} > 1$ if, e.g., the number densities of both UHECRs and neutrinos are peaked at small radii. In what follows, we fix $\mathcal{B} = 1$ and $\tau_{\rm esc} \simeq 2$ Gyr [31], neglecting any dependence on the CR energy that $\tau_{\rm esc}$ (and $\mathcal{B}$) may have. We checked that implementing the $\tau_{\rm esc}$ energy-dependence as in [32] would only slightly (enhance) suppress the (low-energy) high-energy tail of the boosted RνB spectrum, without altering significantly our final results.

We model UHECRs in cluster reservoirs following [31]. For each nucleus $\mathcal{N}$, we write

$$\frac{d\Phi_{\mathcal{N}}}{dE_{\mathcal{N}}} = K_{\mathcal{N}} \left(\frac{E_{\mathcal{N}}^{\max}}{E_{\mathcal{N}}}\right)^{\alpha} e^{-E_{\mathcal{N}}/E_{\mathcal{N}}^{\max}}, \tag{7}$$

where $2 \leq \alpha \leq 2.5$ and $E_{\mathcal{N}}^{\max}/Z_{\mathcal{N}} \simeq 7.69 \times 10^{10}$ GeV, $Z_{\mathcal{N}}$ being the atomic number of $\mathcal{N}$. We checked that varying $E_{\mathcal{N}}^{\max}$ within a factor of up to five from our benchmark choice has a comparable impact, on the detectability of the RνB flux, to varying $2 \leq \alpha \leq 2.5$. We consider the relative nuclear abundances as given in [31] and fix the normalization factors $K_{\mathcal{N}}$ by requiring that the total luminosity emitted from the entire population of CR-reservoirs matches with the one observed at Earth. Concentrating on the energy range $E_{\rm CR}^{\rm ankle} = 5$ EeV $\leq E_{\rm CR} \leq 200$ EeV, approximating the observed extragalactic CR spectrum as a single power-law $d\Phi_{\rm CR}/dE_{\rm CR} \simeq (d\Phi_{\rm CR}/dE_{\rm CR})_{\rm ankle}(E_{\rm CR}^{\rm ankle}/E_{\rm CR})^{2.5}$, with $(d\Phi/dE_{\rm CR})_{\rm ankle} \simeq 10^{-27}$ GeV^{-1} cm^{-2} s^{-1} sr^{-1} [15], and taking as a benchmark value $\alpha = 2.3$ [31], we find $K_{\rm H(He)} \simeq 9.44 \times 10^{-31}(9.52 \times 10^{-32})$ GeV^{-1} cm^{-2} s^{-1} sr^{-1} for ^{1}H (^{4}He), while heavier nuclei are subdominant. We give more details on the normalization procedure in Appendix D.

The resulting total flux on Earth of relic neutrinos upscattered in CR-reservoirs is shown in Fig. 1. We compare it with current observations, limits and future sensitivities, and with the flux of cosmogenic neutrinos arising as secondary products of UHECRs interactions inside reservoirs as computed in [31], because that could constitute a background to our signal. The total flux is obtained by summing over all neutrino mass eigenstates ν_i having nonzero masses m_i, $i = 1, 2, 3$. The upper and lower panels are respectively for a light neutrino mass spectrum with normal ordering (NO) $m_1 < m_2 < m_3$, and inverted ordering (IO) $m_3 < m_1 < m_2$. For NO (IO), the squared mass differences are fixed to $\Delta m_{21}^2 \equiv m_2^2 - m_1^2 = 7.42 \times 10^{-5}$ eV^2 and $\Delta m_{31(23)}^2 \equiv m_{3(2)}^2 - m_{1(3)}^2 = 2.507(2.486) \times 10^{-3}$ eV^2 [71], the sum of neutrino masses saturates the cosmological limit $\sum_i m_i = 0.113(0.145)$ eV [54], and the weighted overdensity is set to $\mathcal{B}\bar{\eta}_\nu = 3 \times 10^8$ for concreteness.

We further note that RνB-UHECRs scatterings could in principle also alter the measured spectrum of UHECRs. While a detailed study goes beyond the purpose of this work, here we simply estimate the mean free path of UHECRs in CR-reservoirs, due to RνB scatterings as $\lambda \sim 1/(\sigma_{\nu \rm CR}\bar{\eta}_\nu n_{\nu,0})$, finding that the R$\nu$B has a smaller impact on UHECRs than the CMB as long as $\bar{\eta}_\nu \lesssim 10^9$.

III. LIMITS AND SENSITIVITIES ON RELIC NEUTRINO OVERDENSITIES

In Fig. 2 we show the limits and sensitivities on the combination $\mathcal{B}\bar{\eta}_\nu$, against the lightest neutrino mass assuming NO (IO) in the upper (lower) panel. We derive them by imposing that our flux line touches the relevant limit/sensitivity curve. These limits and sensitivities are shown as solid curves in Fig. 2 with different colors, depending on the experiment (see the legend in the plot and the caption for more details).

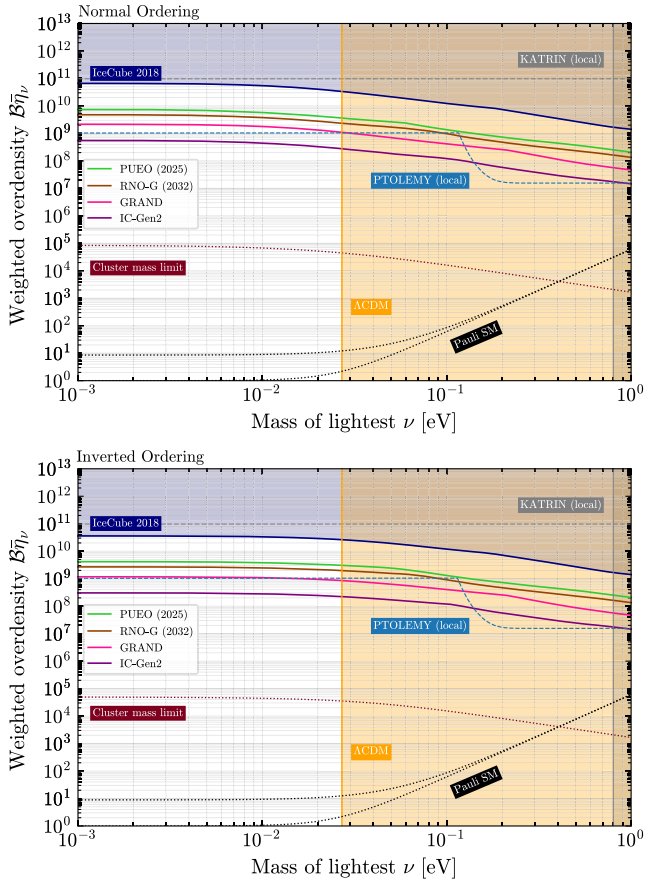

FIG. 2. Limits and sensitivities of $\mathcal{B}\bar{\eta}_\nu$, versus the lightest neutrino mass. Assuming the reference slope $\alpha = 2.3$ in the CR spectrum in CR-reservoirs, and a neutrino mass spectrum with NO (IO) in the upper (lower) panel, we show the 90% CL constraint set by the null-detection at IceCube [21] (blue shaded) and the sensitivities at PUEO (2025) [61], RNO-G (2032) [62], GRAND [64] and IceCube-Gen2 [63] (solid lines, top to bottom). Also shown are: the KATRIN limits on neutrino masses (solid), $m_\nu < 0.8$ eV at 90% CL. [72]; the KATRIN limit on local neutrino overdensities (dashed gray), $\eta_\nu^{\rm Earth} < 9.7 \times 10^{10}$ [9]; the limit on the sum of neutrino masses from DESI, $\sum_i m_i < 0.113(0.145)$ eV at 95% CL assuming ΛCDM [54] (orange shaded); the maximum $\mathcal{B}\bar{\eta}_\nu$ allowed by the Pauli exclusion principle (black dotted, $\mathcal{B} = 1$), respectively for the heaviest (upper line) and lightest (lower line) neutrino; the cluster mass limit (red dotted); the PTOLEMY sensitivity (dashed cyan) on the local overdensity [8]. See the text for further details.

Our limits and sensitivities are compared with the Pauli exclusion principle constraining the number density of gravitationally-bound neutrinos, when no BSM clustering effect is assumed. We compute the local maximum overdensity as prescribed in [11] for a galaxy cluster of

mass $M = 5 \times 10^{15} M_\odot$, assuming a Navarro-Frenk-White (NFW) [73] profile for the surrounding dark matter halo, and then average over the cluster volume. The results of this procedure are shown in dotted black in Fig. 2.

We also evaluate the overdensity $\bar{\eta}_\nu$ for which the RνB mass equals that of the entire galaxy cluster. We consider a NFW dark matter density profile whose virial radius scales as $R_{\rm vir} \sim M^{1/3}$, such that the average mass density in clusters $\rho_{\rm cluster}$ is independent of the cluster mass. In particular, $\rho_{\rm cluster} \approx 200\rho_c$, with $\rho_c \simeq 1.05 \times 10^{-5} h^{-2}$ GeV cm^{-3} the critical density of the Universe and $h \simeq 0.674$ the dimensionless Hubble parameter [74]. We then impose a rough cluster mass limit by requiring $\bar{\eta}_\nu n_{\nu,0} \sum_i m_i \leq \rho_{\rm cluster}$, taking equal averaged overdensity for each neutrino species. The corresponding limit on the weighted overdensity $\mathcal{B}\bar{\eta}_\nu$ can be relaxed for nonuniform neutrino and CR spatial distributions. This is shown in dotted red in Fig. 2.

Finally, we estimate the sensitivity of the proposed PTOLEMY experiment [8] on local neutrino overdensities, considering the configuration where the final $^3\mathrm{He}^+$ is in the bound ground state. Depending on the neutrino mass compared to the experimental resolution Δ (we use $\Delta = 0.05$ eV as reference), the RνB absorption peak can be well-separated from the continuous β-decay spectrum or hidden under it. Accordingly, we require at least $N_{\rm peak} = 10$ events/yr to call a detection in the first situation, or $N_{\rm peak} \gtrsim 3\sqrt{N_{\rm bkg}}$, with $N_{\rm bkg}$ the number of β-decay events/yr in the same energy range in the second. The PTOLEMY sensitivity is shown in dashed cyan in Fig. 2.

For IO and in the hierarchical limit with $m_3 \ll m_1 \lesssim m_2$, there are two heavy and one light neutrino implying a flux that is larger by a factor ~2 with respect to the results in the NO case. Correspondingly, the limits and sensitivities on $\mathcal{B}\bar{\eta}_\nu$ are slightly improved compared to the case of NO. We note, however, that also the cluster mass limit becomes more stringent by an equal amount, for the same reason. In the degenerate limit $m_1 \simeq m_2 \simeq m_3$, the IO case is practically identical to the scenario with NO.

IV. FLAVOR COMPOSITION OF UP-SCATTERED RELIC NEUTRINOS

Neutrinos produced in astrophysical environments typically exhibit precise flavor composition at the source, but neutrino oscillations over astronomical distances tend to homogenize any flavor disparity [75,76].

Instead, the boosted RνB exhibits a peculiar flavor composition. At first, the RνB is evenly distributed among the mass eigenstates, which directly take part in the NC scatterings with UHECRs. The mass eigenstates ν_i then propagate freely and their fluxes $d\Phi_i/dE_\nu$ are preserved. At detection, the probability of observing a massive neutrino ν_i in a flavor $\ell = e, \mu, \tau$ is $\mathcal{P}_{\ell i} = |U_{\ell i}|^2$, with $U_{\ell i}$ being the entries of the Pontecorvo-Maki-Nakagawa-Sakata (PMNS) neutrino mixing matrix [77–79]. Then,

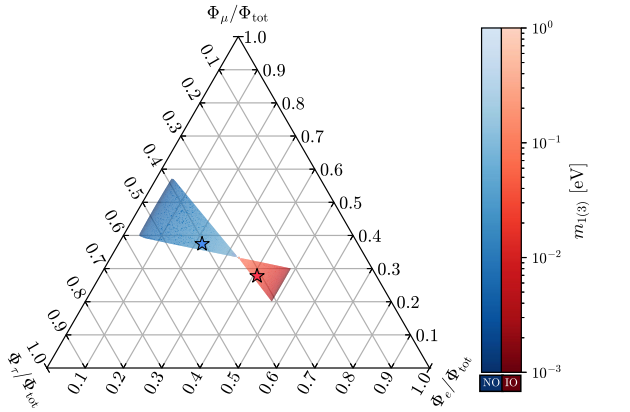

FIG. 3. Flavor composition of the boosted RνB. The blue (red) area is obtained by varying the PMNS matrix entries and squared neutrino mass splittings within the 3σ allowed range [71], assuming NO (IO). Darker regions correspond to lighter $m_{1(3)}$. The stars mark the flavor composition of the boosted RνB for the best-fit values of the neutrino oscillation data and $m_{1(3)}$ saturating the cosmological bounds $\sum_i m_i = 0.113(0.145)$ eV [54] (the flavor composition depends only very slightly on the slope of the CR spectrum).

the flux of boosted neutrinos with flavor ℓ is given by $d\Phi_\ell/dE_\nu = \sum_i |U_{\ell i}|^2 d\Phi_i/dE_\nu$. Clearly, the relative flux in each flavor depends on the neutrino mixing parameters through the PMNS matrix and neutrino masses via the differential flux.

As the fluxes of the different mass eigenstates have distinct energy dependence, the flavor composition of the boosted RνB flux depends on the energy as well. It is nevertheless practical to calculate an integrated flavor ratio $\Phi_\ell/\Phi_{\rm tot} \equiv \sum_i |U_{\ell i}|^2 \Phi_i / \sum_i \Phi_i$. The predicted integrated flavor composition is shown in Fig. 3. In the plot, the parameters of the PMNS matrix are varied within the 3σ ranges allowed by the NuFit 5.2 global analysis of neutrino oscillation data [71,80], while $m_{1(3)}$ in the range $10^{-3} \leq m_{1(3)}/\mathrm{eV} \leq 1$, for NO (IO). As $m_{1(3)}$ increases, the mass eigenstates become nearly degenerate, implying $\Phi_1 \simeq \Phi_2 \simeq \Phi_3$ and an unflavored composition $\Phi_e : \Phi_\mu : \Phi_\tau = 1:1:1$, due to the unitarity of the PMNS matrix. By decreasing $m_{1(3)}$, the mass spectrum becomes hierarchical with $m_1 \lesssim m_2 \ll m_3$ ($m_3 \ll m_1 \lesssim m_2$) with the (two) heaviest neutrino(s) dominating the total flux. In this situation, because of the structure of the PMNS matrix, the flavor flux composition is approximately $0:1:1$ ($2:1:1$) for NO (IO). This could help UHE neutrino observatories discriminate between a boosted RνB signal and other kinds of astrophysical neutrino fluxes [61,64,81–84].

V. CONCLUSIONS

We computed the flux of relic neutrinos up-scattered by UHECRs via SM NC interactions, taking into account the full Q^2-dependence and DIS in the cross section, and the

mixed CR composition. Our results are shown in Fig. 1 for up-scatterings in the MW by UHECRs traveling toward Earth and in galaxy clusters acting as CR-reservoirs. These objects constitute an ideal environment because of the long trapping times of CRs inside them, and indeed lead to the largest RνB up-scattered fluxes. Our calculation is conservative, having not included the hadron-resonances contributions to ν-UHECR scatterings, nor the secondary neutrinos produced by their SM charged-current interactions.

We find that IceCube [21] excludes $\mathcal{B}\bar{\eta}_\nu \gtrsim 10^{10}$ in galaxy clusters, where we weighted the average overdensity $\bar{\eta}_\nu$ by a spatial boost factor $\mathcal{B}$, and that future telescopes [61–64] could possibly detect the boosted RνB for $\mathcal{B}\bar{\eta}_\nu \gtrsim 10^8$, see Fig. 2. These large overdensities require a BSM origin, as could be obtained on the scales of galaxy clusters via, e.g., long-range interactions.

To distinguish a boosted RνB signal from other UHEν fluxes, such as cosmogenic neutrinos, we propose to rely on (i) the shape of the energy spectrum, DIS being crucial in determining the one of the up-scattered RνB, and (ii) the flavor composition, the specific one of the up-scattered RνB being displayed in Fig. 3.

Our study motivates further UHEν searches at telescopes, a direct implementation of RνB-UHECR scatterings in the modeling of CR-reservoirs and sources, and research on how to obtain the sizeable neutrino overdensities required for a potential detection.

ACKNOWLEDGMENTS

We thank Angelo Esposito for precious elucidations on the PTOLEMY experimental set-up, Ke Fang for clarifications on [31], and Silvia Pascoli for useful discussions. We acknowledge the use of computational resources from the parallel computing cluster of the Open Physics Hub ([85]) at the Physics and Astronomy Department in Bologna. J. N. acknowledges hospitality from the Fermilab Theoretical Physics Department. This work was supported in part by the European Union's Horizon research and innovation program under the Marie Skłodowska-Curie Grant Agreements No. 860881-HIDDeN and No. 101086085-ASYMMETRY, by COST (European Cooperation in Science and Technology) via the COST Action COSMIC WISPers CA21106, and by the Italian INFN program on Theoretical Astroparticle Physics.

APPENDIX A: FORM FACTORS OF THE ν-N NEUTRAL CURRENT ELASTIC SCATTERING CROSS SECTION

A detailed derivation of the ν-N elastic scattering cross section can be found in, e.g., [33] (see also [34]). Here, for completeness, we only report the form of the factors A_N and C_N appearing in Eq. (4) of the main text in terms of the momentum transfer Q^2. These are given in terms of the weak neutral current form factors by [33,34]

$$A_N(Q^2) = \frac{Q^2}{m_N^2}\left\{\left(1+\frac{Q^2}{4m_N^2}\right)(G_{\rm A}^{ZN}(Q^2))^2 - \left(1-\frac{Q^2}{4m_N^2}\right)\left[(F_1^{ZN}(Q^2))^2 + \frac{Q^2}{4m_N^2}(F_2^{ZN}(Q^2))^2\right]\right\} \tag{A1}$$

$$C_N(Q^2) = \frac{1}{4}\left[(G_{\rm A}^{ZN}(Q^2))^2 + (F_1^{ZN}(Q^2))^2 + \frac{Q^2}{4m_N^2}(F_2^{ZN}(Q^2))^2\right] \tag{A2}$$

where $F_{1,2}^{ZN}(Q^2) \simeq \pm(1/2)[F_{1,2}^{p}(Q^2) - F_{1,2}^{n}(Q^2)] - 2s_{\rm W}^2 F_{1,2}^{N}\times(Q^2)$, with F_1^N and F_2^N being respectively the Dirac and Pauli electromagnetic form factors for the nucleon $N = n$, p, with the $+(-)$ sign for $p(n)$, $s_{\rm W}^2 \simeq 0.229$ [74] the sine squared of the Weinberg angle, $G_{\rm A}^{Zp}(Q^2) \simeq (1/2)G_{\rm A}(Q^2)$ and $G_{\rm A}^{Zn}(Q^2) \simeq -(1/2)G_{\rm A}(Q^2)$ and $G_{\rm A}(Q^2)$ the axial weak charged current form factor. We have neglected the contributions from the form factors related to strange and heavier quarks, as well as the pseudoscalar contribution (which vanishes exactly in the case of massless neutrinos). It is useful to define also the electric and magnetic form factors respectively as [86–88]

$$G_{\rm E}^N(Q^2) \equiv F_1^N(Q^2) - \frac{Q^2}{4m_N^2}F_2^N(Q^2), \tag{A3}$$

$$G_{\rm M}^N(Q^2) \equiv F_1^N(Q^2) + F_2^N(Q^2). \tag{A4}$$

At zero momentum transfer, i.e., $Q^2 = 0$, we have $G_{\rm E}^p(0) = 1$, $G_{\rm E}^n(0) = 0$, $G_{\rm M}^p(0) = \mu_p/\mu_N$, and $G_{\rm M}^n(0) = \mu_n/\mu_N$, where μ_N is the nuclear magneton, while $\mu_p \simeq 2.79\mu_N$ and $\mu_n \simeq -1.91\mu_N$ are respectively the magnetic moments of the proton and of the neutron [74]. The Q^2-dependence of the electric, magnetic and axial form factors is often fitted experimentally against dipole expressions, namely $G_{\rm E,M}(Q^2) = G_{\rm E,M}(0)(1+Q^2/\Lambda_{\rm E,M}^2)^{-2}$ with $\Lambda_{\rm E,M} \simeq 0.8$ GeV, given in terms of the experimentally measured electric charge and magnetic radii of the proton $\langle r_{\rm E,M}^2\rangle^{1/2} = \sqrt{12}/\Lambda_{\rm E,M} \simeq 0.85$ fm [89,90], while $G_{\rm A}(Q^2) = G_{\rm A}(0)(1+Q^2/m_{\rm A}^2)^{-2}$ with $G_{\rm A}(0) \simeq 1.245$ and $m_{\rm A} \simeq 1.17$ GeV, from measurements of the axial radius $\langle r_{\rm A}^2\rangle^{1/2} = \sqrt{12}/m_{\rm A} \simeq 0.582$ fm [91].

APPENDIX B: NEUTRAL CURRENT DEEP INELASTIC SCATTERING CROSS SECTION

If the center-of-mass energy is sufficiently large, the interaction between a neutrino and a nucleon $N = p$, n takes place with its constituents through DIS. In this section, we derive the NC DIS cross section assuming a parton model with quarks carrying a fraction ξ of the

nucleon's momentum, and then average the results over the quark PDFs. The process is diagrammatically represented below using the TikZ-Feynman package [92].

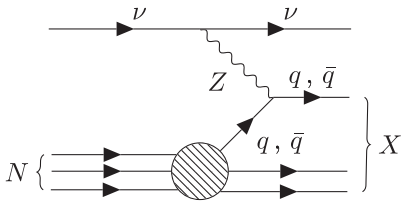

We fix the momenta of the incoming neutrino and quark respectively as $p_\nu = (E_\nu, \vec{p}_\nu)$ and $p_q = (E_q, \vec{p}_q)$. Analogously, for the outgoing neutrino and quarks we define $k_\nu = (E'_\nu, \vec{k}_\nu)$ and $k_q = (E'_q, \vec{k}_q)$, respectively. Furthermore, we neglect the quark masses. The DIS is typically studied in the frame of reference in which the nucleon is at rest $\vec{p}_N = 0$ (LAB), see, e.g., the comprehensive derivation in [33] and references therein (see also [93]). However, we are interested in the frame in which the relic neutrino is at rest instead. Our approach will be that of recovering the DIS cross section in the LAB frame and write it in terms of Lorentz invariants, so to render any change of reference frame immediate. It will prove useful to define also the initial nucleon momentum $p_N = p_q/\xi = (E_N, \vec{p}_N)$ and the 4-momentum transfer $q = p_\nu - k_\nu$. Keeping the same notation as in the main text, we denote the squared centre-of-mass energy and momentum transfer respectively as $s = (p_N + p_\nu)^2$ and $Q^2 = -q^2$. We also define the following Lorentz invariant quantities:

energy transfer

$$\epsilon \equiv \frac{p_N \cdot q}{m_N}; \tag{B1}$$

inelasticity

$$y \equiv \frac{p_N \cdot q}{p_N \cdot p_\nu} = \frac{2\epsilon m_N}{s - m_N^2 - m_\nu^2}; \tag{B2}$$

Bjorken scaling variable

$$x \equiv \frac{Q^2}{2p_N \cdot q} = \frac{Q^2}{(s - m_N^2 - m_\nu^2)y}. \tag{B3}$$

Moreover, we have the following set of relations:

$$Q^2 \overset{\text{LAB}}{=} -2m_\nu^2 + 2E_\nu E'_\nu - 2|\vec{p}_\nu||\vec{k}_\nu|\cos\theta, \tag{B4}$$

$$E_\nu \overset{\text{LAB}}{=} \frac{s - m_N^2 - m_\nu^2}{2m_N}, \tag{B5}$$

$$E'_\nu \overset{\text{LAB}}{=} E_\nu(1 - y), \tag{B6}$$

$$v_{\text{rel}} \overset{\text{LAB}}{=} |\vec{p}_\nu| m_N/(E_\nu E_N), \tag{B7}$$

where θ is the scattering angle in the LAB frame and v_{rel} is the relative velocity between the neutrino and the nucleon. In particular, we have $\partial\cos\theta/\partial x = -m_N E_\nu y/(|\vec{p}_\nu||\vec{k}_\nu|)$ and $\partial E'_\nu/\partial y \overset{\text{LAB}}{=} -E_\nu$, so that

$$\frac{4\pi}{4E_\nu E_N v_{\text{rel}}} \frac{d^3k_\nu}{(2\pi)^3 2E'_\nu} = \frac{y}{8\pi}\left[1 + \mathcal{O}\left(\frac{m_\nu m_N}{p_\nu \cdot p_N}\right)\right] dxdy. \tag{B8}$$

The master formula for the DIS differential cross section can be written as [93]

$$\begin{aligned} d\sigma_{\nu N}^{\text{DIS}} &= \frac{1}{4E_\nu E_N v_{\text{rel}}} \frac{d^3k_\nu}{(2\pi)^3 2E'_\nu} \sum_{a=q,\bar{q}} \int_0^1 d\xi f_a^N(\xi, Q^2) \frac{E_N}{E_a} \int \frac{d^3k_a}{(2\pi)^3 2E'_a} (2\pi)^4 \delta^{(4)}(\xi p_N + q - k_a) |\bar{\mathcal{M}}|^2 \\ &\simeq \frac{G_F^2}{2\pi} \frac{y}{(1 + Q^2/M_Z^2)^2} [p_\nu^\alpha k_\nu^\beta + p_\nu^\beta k_\nu^\alpha - g^{\alpha\beta}(k_\nu \cdot p_\nu) \pm i\varepsilon^{\alpha\beta\gamma\delta} p_{\nu,\gamma} k_{\nu,\delta}] \sum_{a=q,\bar{q}} F_{\alpha\beta}^a dxdy, \end{aligned} \tag{B9}$$

where $+(-)$ applies to neutrinos (antineutrinos); $G_F \simeq 1.167 \times 10^{-5}$ GeV^{-2} is the Fermi weak coupling constant; $|\bar{\mathcal{M}}|^2$ is the squared Feynman amplitude of the neutrino-quark elastic scattering averaged over the initial quark spins; $g^{\alpha\beta} = \text{diag}(1, -1, -1, -1)$ is the Minkowski metric tensor; $\varepsilon^{\alpha\beta\gamma\delta}$ is the totally antisymmetric tensor; $f_{q(\bar{q})}^N$ is the Lorentz scalar PDF for the (anti)quark q ($\bar{q}$) in the nucleon N and we have neglected neutrino masses in comparison with the energies and other mass scales involved. The hadronic tensor $F_{\alpha\beta}^a$ related to (anti)quark $a = q(\bar{q})$ is defined as

$$\begin{aligned} F_{\alpha\beta}^a = \frac{f_a^N(x, Q^2)}{4Q^2} \sum_{\text{spins}} &\langle a(xp_N)|J_\alpha^a|a(k_a)\rangle \\ &\times \langle a(k_a)|J_\beta^{a\dagger}|a(xp_N)\rangle, \end{aligned} \tag{B10}$$

and the neutral quark current (multiplied by the numerator of the Z boson propagator and having factored out the electroweak coupling constant) as

$$J_\alpha^q = \left(g_{\alpha\beta} - \frac{q_\alpha q_\beta}{M_Z^2}\right) \bar{q}\gamma^\beta (g_V^q - g_A^q \gamma_5) q, \tag{B11}$$

where γ^α are the ordinary Dirac gamma matrices, $\gamma^5 = (i/4!)\epsilon_{\alpha\beta\gamma\delta}\gamma^\alpha\gamma^\beta\gamma^\gamma\gamma^\delta$ is the fifth gamma matrix, and the couplings are given by $g_V^{u,c,t} = 1/2 - (4/3)s_W^2$, $g_A^{u,c,t} = 1/2$, $g_V^{d,s,b} = -1/2 + (2/3)s_W^2$ and $g_A^{d,s,b} = -1/2$. We note that $F^a_{\alpha\beta}$ can only depend on the momenta p_N and q and thus decomposes into

$$\begin{aligned} F^a_{\alpha\beta} = &-g_{\alpha\beta}F_1^a + \frac{p_{N\alpha}p_{N\beta}}{m_N^2}\frac{m_N}{\epsilon}F_2^a - i\frac{\epsilon_{\alpha\beta\gamma\delta}p_N^\gamma q^\delta}{2m_N^2}\frac{m_N}{\epsilon}F_3^a \\ &+ \frac{q^\alpha q^\beta}{m_N^2}F_4^a + \frac{p_N^\alpha q^\beta + p_N^\beta q^\alpha}{2m_N^2}F_5^a \\ &+ i\frac{p_N^\alpha q^\beta - p_N^\beta q^\alpha}{2m_N^2}F_6^a. \end{aligned} \tag{B12}$$

With the adopted decomposition of $F^a_{\alpha\beta}$, the quantities F_1^a, F_2^a, F_3^a, F_4^a, F_5^a, and F_6^a are dimensionless. As can be checked, the third line proportional to F_6^a gives vanishing contributions when contracted with the combination of leptonic momenta appearing in the second line of Eq. (B9). The same holds for the F_4^a and F_5^a contributions in the limit of vanishing neutrino masses. Thus, only the terms proportional to F_1^a, F_2^a, and F_3^a are relevant in our calculation. We then get the following expressions for the F_1^a, F_2^a, and F_3^a [33]:

$$F_1^{q(\bar{q})} = \frac{1}{2}[(g_V^q)^2 + (g_A^q)^2]f^N_{q(\bar{q})}(x, Q^2), \tag{B13}$$

$$F_2^{q(\bar{q})} = 2xF_1^{q(\bar{q})} \tag{B14}$$

$$F_3^{q(\bar{q})} = (-)2g_V^q g_A^q f^N_{q(\bar{q})}(x, Q^2). \tag{B15}$$

Plugging the above expressions in Eq. (B9), after contraction of the Lorentz indices, we arrive to [33,34]:

$$\frac{d^2\sigma^{\rm DIS}_{\nu N}}{dxdy} \simeq \frac{G_F^2}{2\pi}\frac{Q^2}{[1+Q^2/M_Z^2]^2}\left[yF_1^{ZN}(x,Q^2) + \frac{1}{xy}\left(1 - y - \frac{m_N^2x^2y^2}{Q^2}\right)F_2^{ZN}(x,Q^2) \pm \left(1 - \frac{y}{2}\right)F_3^{ZN}(x,Q^2)\right], \tag{B16}$$

where $+(-)$ for the scattering with (anti)neutrinos, while $F_1^{ZN} = \sum_{a=q,\bar{q}} F_1^a$, $F_2^{ZN} = \sum_{a=q,\bar{q}} F_2^a$, and $F_3^{ZN} = \sum_{a=q,\bar{q}} F_3^a$. Note that, in the above formula, Q^2 should be given in terms of x, y and s as $Q^2 = (s - m_N^2 - m_\nu^2)xy$. It can be further simplified if we consider the sum of neutrinos and antineutrinos contributions, $\sigma^{\rm DIS}_{(\nu+\bar{\nu})\rm N} = \sigma^{\rm DIS}_{\nu N} + \sigma^{\rm DIS}_{\bar{\nu}N}$:

$$\frac{d^2\sigma^{\rm DIS}_{(\nu+\bar{\nu})\rm N}}{dxdy} \simeq \sum_{a=q,\bar{q}}\frac{G_F^2}{2\pi}\frac{Q^2[(g_V^a)^2 + (g_A^a)^2]f_a^N(x,Q^2)}{[1+Q^2/M_Z^2]^2}\left(y - 2 + \frac{2}{y} - \frac{2m_N^2x^2y}{Q^2}\right). \tag{B17}$$

In the reference frame in which the neutrino is at rest, the variable x can be written as $x = (E_\nu - m_\nu)/(E_N y)$, from which we get $dx/dE_\nu = 1/(E_N y)$. Then, the DIS differential cross section that we need for the boosted neutrino flux calculation is given by

$$\frac{d\sigma^{\rm DIS}_{(\nu+\bar{\nu})\rm N}}{dE_\nu} = \frac{1}{E_N}\int_{y_{\rm min}}^{y_{\rm max}}\frac{dy}{y}\frac{d\sigma^{\rm DIS}_{(\nu+\bar{\nu})\rm N}}{dxdy}, \tag{B18}$$

which leads to the expression given in Eq. (5) of the main text, where, to keep a shorter notation, we have written $d\sigma^{\rm DIS}_{\nu N}$ in place of $d\sigma^{\rm DIS}_{(\nu+\bar{\nu})\rm N}$. As already specified, to evaluate numerically the quark PDFs, we made use of the Python package `parton` and the "CT10" PDF set [35]. The quark PDFs in the considered library are given for $x \geq x_{\rm min} = 10^{-8}$ and in the range $Q^2_{\rm min} = 1.69\ {\rm GeV}^2 \leq Q^2 \leq Q^2_{\rm max} = 10^{10}\ {\rm GeV}^2$. This practically limits our ability to properly estimate the DIS cross section outside the energy range $Q^2_{\rm min}/(2m_\nu) \leq E_\nu - m_\nu \leq \min\{Q^2_{\rm max}/(2m_\nu), T_\nu^{\rm max}(T_N)\}$, where $T_\nu^{\rm max}(T_N)$ is the maximal kinetic energy the neutrino can have after an elastic scattering,

$$T_\nu^{\rm max}(T_N) = \frac{(T_N^2 + 2m_N T_N)}{T_N + (m_N + m_\nu)^2/(2m_\nu)}, \tag{B19}$$

and $T_N \equiv E_N - m_N$ the initial kinetic energy of the incoming nucleon. As an indicative procedure to avoid unphysical discontinuities, we have extrapolated the DIS contribution for $Q^2 \leq Q^2_{\rm min}$ by assuming a linear scaling in Q^2. In practice, this does not affect any of our predictions for the range of E_ν of interest for the UHE neutrino telescopes considered in our study. Finally, we note that the inelasticity parameter lies between $y_{\rm min} = (E_\nu - m_\nu)/E_N$ and $y_{\rm max} = \min\{1, (E_\nu - m_\nu)/(E_N x_{\rm min})\} = 1$.

APPENDIX C: BOOSTED RELIC NEUTRINOS FROM COSMIC RAYS: REVISITED

We revisit the computation of the CR-induced boosted relic neutrino flux discussed in [14], implementing the full cross section with Q^2-dependence of the form factors, the DIS contribution and a mixed CR composition. First, we note that the ES cross section in the low-energy limit $2m_\nu E_N \lesssim m_N^2$ [33] reads:

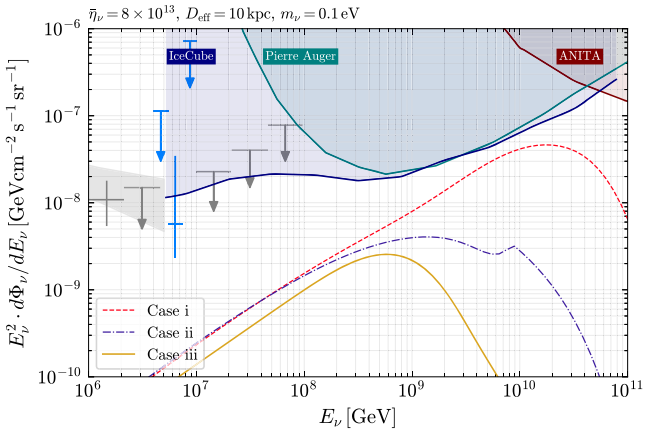

FIG. 4. Comparison between different procedures used to calculate the boosted all-flavor relic neutrino flux according to Eq. (2) of the main text, with $\bar{\eta}_\nu = 8\times10^{13}$, $D_{\rm eff} = 10$ kpc and $m_\nu = 0.1$ eV. The dashed red line corresponds to case (i) for which a low-energy limit of the elastic scattering cross section and a pure proton CR flux are considered; the dot-dashed purple line to case (ii) with a full elastic plus inelastic cross section and a pure proton CR flux; the thick yellow line to case (iii) with a full cross section and a mixed CR composition according to scenario 1 of [15]. See the text for further details. The excluded regions and data points are as in Fig. 1.

$$\frac{d\sigma^{\rm ES}_{\nu N}}{dE_\nu} \simeq \frac{G_F^2(s-m_N^2)^2}{16\pi s T_\nu^{\rm max}(T_N)}[(1-4s_{\rm W}^2)^2 + 3(G_{\rm A}(0))^2], \qquad \text{(C1)}$$

with $T_\nu^{\rm max}(T_N)$ as given in Eq. (B19). The expression in Eq. (C1) resembles the expression reported in [14] in the same limit, apart from an overall $\mathcal{O}(1)$ factor. Our calculation of the cross section differs instead more with respect to the one in [14] for $2m_\nu E_N \gtrsim m_N^2$.

We show in Fig. 4 the neutrino flux computed according to Eq. (2), with $m_\nu = 0.1$ eV, $D_{\rm eff} = 10$ kpc, $\bar{\eta}_\nu = 8\times10^{13}$ roughly saturating the limit given in [14], and different benchmark cases described in what follows. Our choice of $D_{\rm eff}$ is motivated if the neutrino overdensity is localized on a scale of the order of the MW radius.

(i) The red dashed line is obtained by taking the cross section as in (C1) after recasting the all-species CR flux as observed at Earth from [50] in the energy range 10^5 GeV $\lesssim E_{\rm CR} \lesssim 200$ EeV and assuming a pure proton composition from the lowest to the largest energies. With this procedure we obtain results that are comparable (but not overlapping) with those presented in [14].

(ii) The dot-dashed purple line is obtained by considering the full Q^2-dependent cross section as a sum of the elastic and deep inelastic contributions, as discussed in the main text, while keeping the pure proton CR flux as in case (i). We note a suppression compared to case (i) starting from $E_\nu \sim$ EeV due to the form factors $A_N(Q^2)$ and $C_N(Q^2)$ of the elastic cross section, as well as a kick at $E_\nu \sim 10$ EeV because of the DIS.

(iii) The thick yellow curve is obtained by considering the full cross section as in case (ii) and a mixed composition for the CR flux according to the analysis presented in [15]. Concentrating on the extragalactic contribution only, we considered this flux in the energy range 10^8 GeV $\lesssim E_{\rm CR} \lesssim 200$ EeV. For definiteness, we focused on the scenario 1 described in [15], in which the proton composition gets suppressed earlier compared to heavier nuclei, thus implying an attenuation of the boosted relic neutrino flux.

We point out that the analogous flux in Fig. 1 is obtained as in case (iii), but considering three neutrino species with masses that saturate the cosmological bound [54]—while that in Fig. 4 is for three degenerate neutrinos with reference mass $m_\nu = 0.1$ eV—and starting the integration from $E_{\rm CR}^{\rm ankle}$ to remain conservative on the galactic-to-extragalactic transition.

We find that the implementation of the full momentum transfer dependence of the neutrino-nucleus cross section, the deep inelastic scattering contribution and a mixed CR composition, leads to a boosted relic neutrino flux suppressed significantly with respect to what reported in [14], and, correspondingly, the bounds on the local neutrino overdensity are weakened by an overall $\mathcal{O}(10)$ factor.

APPENDIX D: NORMALIZATION OF THE COSMIC RAY FLUX INSIDE GALAXY CLUSTERS

We discuss here the normalization procedure that we followed for our estimate of the CR flux within galaxy clusters acting as CR-reservoirs, i.e., to determine the function $d\Phi_{\rm CR}/dE_{\rm CR}$ entering Eq. (2) of the main text. We remind that Eq. (2) is intended to be a sum over all species $\mathcal{N}$ constituting CRs, where the dependence on $\mathcal{N}$ is contained both in the flux and in the differential cross section. Concerning the flux, one could proceed by summing the contribution from all CR-reservoirs in the entire Universe, but this requires knowledge on details of the population of clusters that is not really necessary if one assumes that most UHECR observed on Earth originate in these CR-reservoirs. Therefore, under this assumption and as we explain below, we extract the flux from [31], where it has been determined by comparison with the observed UHECR.

We rewrite here the flux of cosmic nucleus $\mathcal{N}$ as given in [31] and as used in our main analysis

$$\frac{d\Phi_\mathcal{N}}{dE_\mathcal{N}} = K_\mathcal{N}\left(\frac{R_{\rm max}}{R}\right)^\alpha e^{-R/R_{\rm max}}. \qquad \text{(D1)}$$

where the rigidity parameter R is defined as $R \equiv E_\mathcal{N}/(Z_\mathcal{N} q_e)$, q_e being the electric charge unit, with $R_{\rm max} = 2\times10^{21}/26$ eV [31] (for convenience, we absorb the

electric charge q_e in the definition of R so that it is measured in eV rather than V). According to [31], at fixed R the chemical composition of $E_{\mathcal{N}}^2 d\Phi_{\mathcal{N}}/dE_{\mathcal{N}}$ is (0.625, 0.252, 0.053, 0.009, 0.124) for (^{1}H, ^{4}He, CNO, ^{28}Si, ^{56}Fe) respectively (as reference for CNO we have considered ^{14}N only). Thus, at fixed R, we have

$$E_{\mathcal{N}}^2 \frac{d\Phi_{\mathcal{N}}}{dE_{\mathcal{N}}} = Z_{\mathcal{N}}^2 K_{\mathcal{N}} R^2 \left(\frac{R_{\rm max}}{R}\right)^{\alpha} e^{-R/R_{\rm max}}, \qquad \text{(D2)}$$

so that the aforementioned proportions are reflected in the ratios of $Z_{\mathcal{N}}^2 K_{\mathcal{N}}$. Therefore, $K_{\mathcal{N}} \equiv (C_{\rm N}/Z_{\rm N}^2) K_{\rm H}$, with $C_{\rm He} \simeq 0.4032$, $C_{\rm N} \simeq 0.0848$, $C_{\rm Si} \simeq 0.0144$, and $C_{\rm Fe} \simeq 0.1984$. The only parameter left to determine is K_H, which we fix by requiring that the luminosity emitted from the population of CR-reservoirs matches with the one observed at Earth, by, e.g., Pierre Auger above the ankle. More specifically, we impose

$$\sum_{\mathcal{N}} \int_{E_{\rm CR}^{\rm ankle}}^{E_{\rm CR}^{\rm max}} dE_{\mathcal{N}} E_{\mathcal{N}} \frac{d\Phi_{\mathcal{N}}}{dE_{\mathcal{N}}} = \int_{E_{\rm CR}^{\rm ankle}}^{E_{\rm CR}^{\rm max}} dE_{\rm CR} E_{\rm CR} \frac{d\Phi_{\rm CR}}{dE_{\rm CR}}, \qquad \text{(D3)}$$

where the CR flux at Earth is taken from [94] to be $d\Phi_{\rm CR}/dE_{\rm CR} \simeq (d\Phi_{\rm CR}/dE_{\rm CR})_{\rm ankle} (E_{\rm CR}^{\rm ankle}/E_{\rm CR})^{2.5}$, with $(d\Phi/dE_{\rm CR})_{\rm ankle} \simeq 10^{-27}$ GeV^{-1} cm^{-2} s^{-1} sr^{-1}, within the range $E_{\rm CR}^{\rm ankle} = 5$ EeV $\leq E_{\rm CR} \leq E_{\rm CR}^{\rm max} = 200$ EeV. The CR flux observed at Pierre Auger and reported in [94] is actually more complicated than the single power-law considered above, including changes in the slopes at and above the ankle, mixed composition and a suppression at ~50 EeV. We have checked, however, that such additional features do not change appreciably the value of the integral in the right-hand-side of Eq. (D3), to which the shape at lower energies dominates. The integral on the left-hand-side can be computed analytically as follows:

$$\begin{aligned}
\sum_{\mathcal{N}} \int_{E_{\rm CR}^{\rm ankle}}^{E_{\rm CR}^{\rm max}} dE_{\mathcal{N}} E_{\mathcal{N}} \frac{d\Phi_{\mathcal{N}}}{dE_{\mathcal{N}}} &= K_{\rm H} \sum_{\mathcal{N}} \frac{C_{\mathcal{N}}}{Z_{\mathcal{N}}^2} \int_{E_{\rm CR}^{\rm ankle}}^{E_{\rm CR}^{\rm max}} dE_{\mathcal{N}} E_{\mathcal{N}} \left(\frac{E_{\mathcal{N}}^{\rm max}}{E_{\mathcal{N}}}\right)^{\alpha} e^{-E_{\mathcal{N}}/E_{\mathcal{N}}^{\rm max}} \\
&= K_{\rm H} \sum_{\mathcal{N}} C_{\mathcal{N}} R_{\rm max}^2 \int_{E_{\rm CR}^{\rm ankle}/(Z_{\mathcal{N}} R_{\rm max})}^{E_{\rm CR}^{\rm max}/(Z_{\mathcal{N}} R_{\rm max})} dx\, x^{1-\alpha} e^{-x} \\
&= K_{\rm H} \sum_{\mathcal{N}} C_{\mathcal{N}} R_{\rm max}^2 \left[\Gamma\left(2-\alpha, \frac{E_{\rm CR}^{\rm ankle}}{Z_{\mathcal{N}} R_{\rm max}}\right) - \Gamma\left(2-\alpha, \frac{E_{\rm CR}^{\rm max}}{Z_{\mathcal{N}} R_{\rm max}}\right)\right], \qquad \text{(D4)}
\end{aligned}$$

where $\Gamma(a, z)$ is the upper incomplete gamma function. For different values of the slope α, we find the normalization factors listed in Table I. These normalization factors *de facto* encode all the information about CR-reservoirs (distance, spatial distribution, CR-spectrum escaping them), that is not needed for our purposes as long as one assumes (as done in [31]) that most UHECRs observed on Earth originate from CR-reservoirs.

TABLE I. Flux normalization factors for each nuclear species considered and different benchmark values of α. All listed values are in units of GeV^{-1} cm^{-2} s^{-1} sr^{-1}.

Normalization factors			
	$\alpha = 2$	$\alpha = 2.3$	$\alpha = 2.5$
$K_{\rm H}$	1.94×10^{-30}	9.44×10^{-31}	5.20×10^{-31}
$K_{\rm He}$	1.96×10^{-31}	9.52×10^{-32}	5.24×10^{-32}
$K_{\rm N}$	3.36×10^{-33}	1.63×10^{-33}	8.99×10^{-34}
$K_{\rm Si}$	1.43×10^{-34}	6.94×10^{-35}	3.82×10^{-35}
$K_{\rm Fe}$	5.70×10^{-34}	2.77×10^{-34}	1.52×10^{-34}

[1] Julien Lesgourgues, Gianpiero Mangano, Gennaro Miele, and Sergio Pastor, *Neutrino Cosmology* (Cambridge University Press, Cambridge, England, 2013).

[2] N. Aghanim *et al.* (Planck Collaboration), Planck 2018 results. VI. Cosmological parameters, Astron. Astrophys. **641**, A6 (2020); **652**, C4(E) (2021).

[3] Gary Steigman, Neutrinos and big bang nucleosynthesis, Adv. High Energy Phys. **2012**, 268321 (2012).

[4] Martin Bauer and Jack D. Shergold, Limits on the cosmic neutrino background, J. Cosmol. Astropart. Phys. 01 (2023) 003.

[5] M. G. Betti *et al.* (PTOLEMY Collaboration), Neutrino physics with the PTOLEMY project: Active neutrino

properties and the light sterile case, J. Cosmol. Astropart. Phys. 07 (2019) 047.
[6] A. Apponi *et al.*, Implementation and optimization of the PTOLEMY transverse drift electromagnetic filter, J. Instrum. **17**, P05021 (2022).
[7] Yevheniia Cheipesh, Vadim Cheianov, and Alexey Boyarsky, Navigating the pitfalls of relic neutrino detection, Phys. Rev. D **104**, 116004 (2021).
[8] A. Apponi *et al.* (PTOLEMY Collaboration), Heisenberg's uncertainty principle in the PTOLEMY project: A theory update, Phys. Rev. D **106**, 053002 (2022).
[9] M. Aker *et al.*, New constraint on the local relic neutrino background overdensity with the first KATRIN data runs, Phys. Rev. Lett. **129**, 011806 (2022).
[10] Yu-Dai Tsai, Joshua Eby, Jason Arakawa, Davide Farnocchia, and Marianna S. Safronova, OSIRIS-REx constraints on local dark matter and cosmic neutrino profiles, J. Cosmol. Astropart. Phys. 02 (2024) 029.
[11] Andreas Ringwald and Yvonne Y. Y. Wong, Gravitational clustering of relic neutrinos and implications for their detection, J. Cosmol. Astropart. Phys. 12 (2004) 005.
[12] Tetsuya Hara and Humitaka Sato, Scattering of the cosmic neutrinos by high energy cosmic rays, Prog. Theor. Phys. **64**, 1089 (1980).
[13] Tetsuya Hara and Humitaka Sato, Elastic and inelastic scattering of the relic neutrinos by high-energy cosmic rays, Prog. Theor. Phys. **65**, 477 (1981).
[14] Mar Císcar-Monsalvatje, Gonzalo Herrera, and Ian M. Shoemaker, Upper limits on the cosmic neutrino background from cosmic rays, Phys. Rev. D **110**, 063036 (2024).
[15] A. Abdul Halim *et al.* (Pierre Auger Collaboration), Constraining the sources of ultra-high-energy cosmic rays across and above the ankle with the spectrum and composition data measured at the Pierre Auger Observatory, J. Cosmol. Astropart. Phys. 05 (2023) 024.
[16] R. U. Abbasi *et al.* (Telescope Array Collaboration), Mass composition of ultrahigh-energy cosmic rays with the telescope array surface detector data, Phys. Rev. D **99**, 022002 (2019).
[17] Daniele Fargion, B. Mele, and A. Salis, Ultrahigh-energy neutrino scattering onto relic light neutrinos in galactic halo as a possible source of highest energy extragalactic cosmic rays, Astrophys. J. **517**, 725 (1999).
[18] Thomas J. Weiler, Cosmic ray neutrino annihilation on relic neutrinos revisited: A mechanism for generating air showers above the Greisen-Zatsepin-Kuzmin cutoff, Astropart. Phys. **11**, 303 (1999).
[19] Jack Franklin, Ivan Martinez-Soler, Yuber F. Perez-Gonzalez, and Jessica Turner, Constraints on the cosmic neutrino background from NGC 1068, arXiv:2404.02202.
[20] Birgit Eberle, Andreas Ringwald, Liguo Song, and Thomas J. Weiler, Relic neutrino absorption spectroscopy, Phys. Rev. D **70**, 023007 (2004).
[21] M. G. Aartsen *et al.* (IceCube Collaboration), Differential limit on the extremely-high-energy cosmic neutrino flux in the presence of astrophysical background from nine years of IceCube data, Phys. Rev. D **98**, 062003 (2018).
[22] Alexander Aab *et al.* (Pierre Auger Collaboration), Probing the origin of ultra-high-energy cosmic rays with neutrinos in the EeV energy range using the Pierre Auger Observatory, J. Cosmol. Astropart. Phys. 10 (2019) 022.
[23] Vedran Brdar, P. S. Bhupal Dev, Ryan Plestid, and Amarjit Soni, A new probe of relic neutrino clustering using cosmogenic neutrinos, Phys. Lett. B **833**, 137358 (2022).
[24] Kyrylo Bondarenko, Alexey Boyarsky, Josef Pradler, and Anastasia Sokolenko, Best-case scenarios for neutrino capture experiments, J. Cosmol. Astropart. Phys. 10 (2023) 026.
[25] Alexei Yu. Smirnov and Xun-Jie Xu, Neutrino bound states and bound systems, J. High Energy Phys. 08 (2022) 170.
[26] H. J. Volk, F. A. Aharonian, and D. Breitschwerdt, The nonthermal energy content and gamma-ray emission of starburst galaxies and clusters of galaxies, Space Sci. Rev. **75**, 279 (1996).
[27] V. S. Berezinsky, P. Blasi, and V. S. Ptuskin, Clusters of galaxies as a storage room for cosmic rays, Astrophys. J. **487**, 529 (1997).
[28] Kohta Murase, Susumu Inoue, and Shigehiro Nagataki, Cosmic rays above the second knee from clusters of galaxies and associated high-energy neutrino emission, Astrophys. J. **689**, L105 (2008).
[29] K. Kotera, D. Allard, K. Murase, J. Aoi, Y. Dubois, T. Pierog, and S. Nagataki, Propagation of ultrahigh energy nuclei in clusters of galaxies: Resulting composition and secondary emissions, Astrophys. J. **707**, 370 (2009).
[30] Kohta Murase and John F. Beacom, Galaxy clusters as reservoirs of heavy dark matter and high-energy cosmic rays: Constraints from neutrino observations, J. Cosmol. Astropart. Phys. 02 (2013) 028.
[31] Ke Fang and Kohta Murase, Linking high-energy cosmic particles by black hole jets embedded in large-scale structures, Nat. Phys. **14**, 396 (2018).
[32] Antonio Condorelli, Jonathan Biteau, and Remi Adam, Impact of galaxy clusters on the propagation of ultrahigh-energy cosmic rays, Astrophys. J. **957**, 80 (2023).
[33] Carlo Giunti and Chung W. Kim, *Fundamentals of Neutrino Physics and Astrophysics* (Oxford University Press, Oxford, UK, 2007).
[34] J. A. Formaggio and G. P. Zeller, From eV to EeV: Neutrino cross sections across energy scales, Rev. Mod. Phys. **84**, 1307 (2012).
[35] Hung-Liang Lai, Marco Guzzi, Joey Huston, Zhao Li, Pavel M. Nadolsky, Jon Pumplin, and C. P. Yuan, New parton distributions for collider physics, Phys. Rev. D **82**, 074024 (2010).
[36] Daniel Z. Freedman, David N. Schramm, and David L. Tubbs, The weak neutral current and its effects in stellar collapse, Annu. Rev. Nucl. Part. Sci. **27**, 167 (1977).
[37] R. P. Feynman, M. Kislinger, and F. Ravndal, Current matrix elements from a relativistic quark model, Phys. Rev. D **3**, 2706 (1971).
[38] Dieter Rein and Lalit M. Sehgal, Neutrino excitation of baryon resonances and single pion production, Ann. Phys. (N.Y.) **133**, 79 (1981).
[39] Stefano Gabici, Carmelo Evoli, Daniele Gaggero, Paolo Lipari, Philipp Mertsch, Elena Orlando, Andrew Strong, and Andrea Vittino, The origin of Galactic cosmic rays: Challenges to the standard paradigm, Int. J. Mod. Phys. D **28**, 1930022 (2019).

[40] Julia Becker Tjus and Lukas Merten, Closing in on the origin of Galactic cosmic rays using multimessenger information, Phys. Rep. **872**, 1 (2020).
[41] S. Thoudam, J. P. Rachen, A. van Vliet, A. Achterberg, S. Buitink, H. Falcke, and J. R. Hörandel, Cosmic-ray energy spectrum and composition up to the ankle: The case for a second Galactic component, Astron. Astrophys. **595**, A33 (2016).
[42] Rafael Alves Batista *et al.*, Open questions in cosmic-ray research at ultrahigh energies, Front. Astron. Space Sci. **6**, 23 (2019).
[43] Alexander Aab *et al.* (Pierre Auger Collaboration), Cosmic-ray anisotropies in right ascension measured by the Pierre Auger Observatory, Astrophys. J. **891**, 142 (2020).
[44] A. Coleman *et al.*, Ultra high energy cosmic rays the intersection of the cosmic and energy frontiers, Astropart. Phys. **149**, 102819 (2023).
[45] R. U. Abbasi *et al.* (HiRes Collaboration), A study of the composition of ultrahigh energy cosmic rays using the high resolution fly's eye, Astrophys. J. **622**, 910 (2005).
[46] R. Aloisio, V. Berezinsky, and P. Blasi, Ultra high energy cosmic rays: Implications of Auger data for source spectra and chemical composition, J. Cosmol. Astropart. Phys. 10 (2014) 020.
[47] R. U. Abbasi *et al.*, Study of ultra-high energy cosmic ray composition using telescope array's middle drum detector and surface array in hybrid mode, Astropart. Phys. **64**, 49 (2015).
[48] R. U. Abbasi *et al.* (Telescope Array Collaboration), The cosmic-ray composition between 2 PeV and 2 EeV observed with the TALE detector in monocular mode, Astrophys. J. **909**, 178 (2021).
[49] A. Abdul Halim *et al.* (Pierre Auger Collaboration), Constraining models for the origin of ultra-high-energy cosmic rays with a novel combined analysis of arrival directions, spectrum, and composition data measured at the Pierre Auger Observatory, J. Cosmol. Astropart. Phys. 01 (2024) 022.
[50] Xing-Jian Lv, Xiao-Jun Bi, Kun Fang, Yi-Qing Guo, Hui-Hai He, Ling-Ling Ma, Peng-Fei Yin, Qiang Yuan, and Meng-Jie Zhao, Precise measurement of the cosmic-ray spectrum and $\langle \ln A \rangle$ by LHAASO—Connecting the Galactic to the extragalactic components, arXiv:2403.11832.
[51] Gang Guo, Yue-Lin Sming Tsai, Meng-Ru Wu, and Qiang Yuan, Elastic and inelastic scattering of cosmic-rays on sub-GeV dark matter, Phys. Rev. D **102**, 103004 (2020).
[52] Chen Xia, Yan-Hao Xu, and Yu-Feng Zhou, Production and attenuation of cosmic-ray boosted dark matter, J. Cosmol. Astropart. Phys. 02 (2022) 028.
[53] R. Xu *et al.* (CDEX Collaboration), Constraints on sub-GeV dark matter boosted by cosmic rays from the CDEX-10 experiment at the China Jinping Underground Laboratory, Phys. Rev. D **106**, 052008 (2022).
[54] A. G. Adame *et al.* (DESI Collaboration), DESI 2024 VI: Cosmological constraints from the measurements of baryon acoustic oscillations, arXiv:2404.03002.
[55] M. G. Aartsen *et al.* (IceCube Collaboration), Characteristics of the diffuse astrophysical electron and tau neutrino flux with six years of IceCube high energy cascade data, Phys. Rev. Lett. **125**, 121104 (2020).
[56] M. G. Aartsen *et al.* (IceCube Collaboration), Detection of a particle shower at the Glashow resonance with IceCube, Nature (London) **591**, 220 (2021); **592**, E11 (2021).
[57] R. Abbasi *et al.* (IceCube Collaboration), The IceCube high-energy starting event sample: Description and flux characterization with 7.5 years of data, Phys. Rev. D **104**, 022002 (2021).
[58] R. Abbasi *et al.*, Characterization of the astrophysical diffuse neutrino flux using starting track events in IceCube, Phys. Rev. D **110**, 022001 (2024).
[59] KM3NeT Collaboration, Differential sensitivity of the KM3NeT/ARCA detector to a diffuse neutrino flux and to point-like source emission: Exploring the case of the starburst galaxies, Astropart. Phys. **162**, 102990 (2024).
[60] P. W. Gorham *et al.* (ANITA Collaboration), Constraints on the ultrahigh-energy cosmic neutrino flux from the fourth flight of ANITA, Phys. Rev. D **99**, 122001 (2019).
[61] Q. Abarr *et al.* (PUEO Collaboration), The payload for ultrahigh energy observations (PUEO): A white paper, J. Instrum. **16**, P08035 (2021).
[62] Marco Stein Muzio *et al.* (RNO-G Collaboration), Multi-messenger potential of the radio neutrino observatory in Greenland, Proc. Sci. ICRC2023 (**2023**) 1485 [arXiv:2308.07224].
[63] Rasha Abbasi *et al.* (IceCube-Gen2 Collaboration), Sensitivity studies for the IceCube-Gen2 radio array, Proc. Sci. ICRC2021 (**2021**) 1183 [arXiv:2107.08910].
[64] Jaime Álvarez-Muñiz *et al.* (GRAND Collaboration), The giant radio array for neutrino detection (GRAND): Science and design, Sci. China Phys. Mech. Astron. **63**, 219501 (2020).
[65] Tadeusz Wibig and Arnold W. Wolfendale, Heavy cosmic ray nuclei from extragalactic sources above "The Ankle", Open Astron. J. **2**, 95 (2009).
[66] Andrew M. Taylor, Markus Ahlers, and Felix A. Aharonian, The need for a local source of UHECR nuclei, Phys. Rev. D **84**, 105007 (2011).
[67] Silvia Mollerach and Esteban Roulet, Ultrahigh energy cosmic rays from a nearby extragalactic source in the diffusive regime, Phys. Rev. D **99**, 103010 (2019).
[68] Rodrigo Guedes Lang, Andrew M. Taylor, Markus Ahlers, and Vitor de Souza, Revisiting the distance to the nearest ultrahigh energy cosmic ray source: Effects of extragalactic magnetic fields, Phys. Rev. D **102**, 063012 (2020).
[69] Pavlo Plotko, Arjen van Vliet, Xavier Rodrigues, and Walter Winter, Differences between the Pierre Auger Observatory and Telescope Array Spectra: Systematic effects or indication of a local source of ultra-high-energy cosmic rays?, Astrophys. J. **953**, 129 (2023).
[70] Gianfranco Brunetti and Thomas W. Jones, Cosmic rays in galaxy clusters and their nonthermal emission, Int. J. Mod. Phys. D **23**, 1430007 (2014).
[71] Ivan Esteban, M. C. Gonzalez-Garcia, Michele Maltoni, Thomas Schwetz, and Albert Zhou, The fate of hints: Updated global analysis of three-flavor neutrino oscillations, J. High Energy Phys. 09 (2020) 178.
[72] M. Aker *et al.* (KATRIN Collaboration), Direct neutrino-mass measurement with sub-electronvolt sensitivity, Nat. Phys. **18**, 160 (2022).

[73] Julio F. Navarro, Carlos S. Frenk, and Simon D. M. White, A universal density profile from hierarchical clustering, Astrophys. J. **490**, 493 (1997).
[74] R. L. Workman and Others (Particle Data Group), Review of particle physics, Prog. Theor. Exp. Phys. **2022**, 083C01 (2022).
[75] Andrea Palladino and Francesco Vissani, The natural parameterization of cosmic neutrino oscillations, Eur. Phys. J. C **75**, 433 (2015).
[76] Mauricio Bustamante, John F. Beacom, and Walter Winter, Theoretically palatable flavor combinations of astrophysical neutrinos, Phys. Rev. Lett. **115**, 161302 (2015).
[77] B. Pontecorvo, Mesonium and anti-mesonium, Sov. Phys. JETP **6**, 429 (1957).
[78] B. Pontecorvo, Inverse beta processes and nonconservation of lepton charge, Sov. Phys. JETP **34**, 247 (1957).
[79] Ziro Maki, Masami Nakagawa, and Shoichi Sakata, Remarks on the unified model of elementary particles, Prog. Theor. Phys. **28**, 870 (1962).
[80] NuFit 5.2, http://www.nu-fit.org.
[81] M. G. Aartsen *et al.* (IceCube Collaboration), Flavor ratio of astrophysical neutrinos above 35 TeV in IceCube, Phys. Rev. Lett. **114**, 171102 (2015).
[82] Andrea Palladino, The flavor composition of astrophysical neutrinos after 8 years of IceCube: An indication of neutron decay scenario?, Eur. Phys. J. C **79**, 500 (2019).
[83] M. G. Aartsen *et al.* (IceCube-Gen2 Collaboration), IceCube-Gen2: The window to the extreme Universe, J. Phys. G **48**, 060501 (2021).
[84] Alan Coleman, Oscar Ericsson, Mauricio Bustamante, and Christian Glaser, The flavor composition of ultra-high-energy cosmic neutrinos: Measurement forecasts for in-ice radio-based EeV neutrino telescopes, Phys. Rev. D **110**, 023044 (2024).
[85] https://site.unibo.it/openphysicshub/en.
[86] F. J. Ernst, R. G. Sachs, and K. C. Wali, Electromagnetic form factors of the nucleon, Phys. Rev. **119**, 1105 (1960).
[87] L. N. Hand, D. G. Miller, and Richard Wilson, Electric and magnetic form factors of the nucleon, Rev. Mod. Phys. **35**, 335 (1963).
[88] C. F. Perdrisat, V. Punjabi, and M. Vanderhaeghen, Nucleon electromagnetic form factors, Prog. Part. Nucl. Phys. **59**, 694 (2007).
[89] J. M. Alarcón, D. W. Higinbotham, and C. Weiss, Precise determination of the proton magnetic radius from electron scattering data, Phys. Rev. C **102**, 035203 (2020).
[90] Haiyan Gao and Marc Vanderhaeghen, The proton charge radius, Rev. Mod. Phys. **94**, 015002 (2022).
[91] Constantia Alexandrou, Simone Bacchio, Martha Constantinou, Jacob Finkenrath, Roberto Frezzotti, Bartosz Kostrzewa, Giannis Koutsou, Gregoris Spanoudes, and Carsten Urbach (Extended Twisted Mass Collaboration), Nucleon axial and pseudoscalar form factors using twisted-mass fermion ensembles at the physical point, Phys. Rev. D **109**, 034503 (2024).
[92] Joshua Ellis, TikZ-Feynman: Feynman diagrams with TikZ, Comput. Phys. Commun. **210**, 103 (2017).
[93] Michael E. Peskin and Daniel V. Schroeder, *An Introduction to Quantum Field Theory* (Addison-Wesley, Reading, USA, 1995).
[94] Alexander Aab *et al.* (Pierre Auger Collaboration), Features of the energy spectrum of cosmic rays above 2.5×10^{18} eV using the Pierre Auger Observatory, Phys. Rev. Lett. **125**, 121106 (2020).